On differences in the equation-of-state for a selection of seven representative mammalian tissue analogue materials

G.J. Appleby-Thomas, B. Fitzmaurice, A. Hameed, J. Painter, M. Gibson, D.C. Wood, R. Hazael, P.J. Hazell

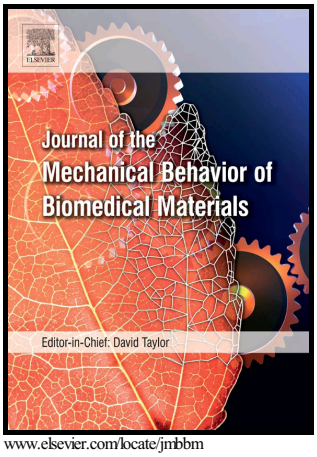

www.elsevier.com/locate/jmbbm

PII: S1751-6161(17)30442-3
DOI: https://doi.org/10.1016/j.jmbbm.2017.10.012
Reference: JMBBM2532

To appear in: *Journal of the Mechanical Behavior of Biomedical Materials*

Received date: 18 July 2017
Revised date: 3 October 2017
Accepted date: 8 October 2017

Cite this article as: G.J. Appleby-Thomas, B. Fitzmaurice, A. Hameed, J. Painter, M. Gibson, D.C. Wood, R. Hazael and P.J. Hazell, On differences in the equation-of-state for a selection of seven representative mammalian tissue analogue materials, *Journal of the Mechanical Behavior of Biomedical Materials,* https://doi.org/10.1016/j.jmbbm.2017.10.012

Journal of the Mechanical Behavior of Biomedical Materials
Volume 77, January 2018, pp. 586-593

On differences in the equation-of-state for a selection of seven representative mammalian tissue analogue materials

G. J. Appleby-Thomas[a), c)], B. Fitzmaurice[a)], A. Hameed[a)], J. Painter[a)], M. Gibson[a)], D. C. Wood[1)], R. Hazael[a)] and P. J. Hazell[b)]

[a)]Centre for Defence Engineering, Cranfield Defence and Security, Cranfield University, Shrivenham, Swindon, SN6 8LA, UK.

[b)]School of Engineering and Information Technology, The University of New South Wales, Canberra, ACT 2600, Australia.

Abstract

Tissue analogues employed for ballistic purposes are often monolithic in nature, e.g. ballistic gelatin and soap, etc. However, such constructs are not representative of real-world biological systems. Further, ethical considerations limit the ability to test with real-world tissues. This means that availability and understanding of accurate tissue simulants is of key importance. Here, the shock response of a wide range of ballistic simulants (ranging from dermal (protective / bulk) through to skeletal simulant materials) determined via plate-impact experiments are discussed, with a particular focus on the classification of the behaviour of differing simulants into groups that exhibit a similar response under high strain-rate loading. Resultant Hugoniot equation-of-state data (U_s-u_p; P-v) provides appropriate feedstock materials data for future hydrocode simulations of ballistic impact events.

1. Introduction

Ballistic testing is necessary in order to optimise protection (armour) against differing threats. However, in order for such tests to be accurate, it is important that targets sitting behind protective materials should also be able to reproduce real-world effects as accurately as possible. Access to appropriate tissue analogues for such applications is therefore of particular importance, primarily due to issues of target

[c)] Author to whom correspondence should be addressed. Tel.: +44 (0) 1793 785731. Electronic mail: g.applebythomas@cranfield.ac.uk.

material consistency and ethical constraints. Despite this important role, the majority of tissue simulants currently in use are relatively simplistic in nature. As an example, both Ballistics Gelatin [1, 2] and Soap [3] are comprised of a single phase, making them essentially bulk (monolithic) tissue analogues. Whereas, real-world tissue-based structures such as limbs are significantly more complex with multiple elements (skeletal, muscular, adipose, etc) present. Further, physical ballistic testing is inherently both resource and time intensive. To this end, it is becoming common practise to compliment experimental ballistics trials with numerical simulations – for example, employing explicit dynamic hydrocodes. The accuracy of the outputs from such simulations is, however, heavily dependent on the quality of the fundamental target (tissue) materials data employed. To this end, understanding of material hydrodynamic and constitutive equations-of-state to enable complimentary simulations is a key requirement if tissue analogues are to be successfully employed in real-world ballistic tests.

A number of studies have already been undertaken at low-medium strain-rates ($<10^4$ /s). At relatively low strain rates, Comley and Fleck [4] investigated the toughness of porcine adipose tissue via a "trouser tear test". This was undertaken with a tensile testing machine at crosshead speeds of just 0.01-10 mm/s. Materials toughness was correlated to two key components of underlying structure. Essentially, energy absorption was linked to a collagen-based reinforcement membrane surrounding lipid-filled cells (adipocytes), with additional secondary toughness contributions from a network of surrounding collagen (known as interlobular septa). In a study more focused on bulk material properties, Jussila et al. [5] carried out a series of ballistic tests using lead spheres of 4.5-mm diameter, with these experiments focused incident on different skin simulants covering gelatin blocks. Via comparison to literature data on penetration threshold velocity, tensile strength and elongation at break for human skin (from cadavers), an optimal skin simulant of approximately 1-mm thick chrome-tanned leather was identified.

However, despite these and other studies [6-8], there continues to be a relative paucity in the literature of fundamental high strain-rate (hydrodynamic) tissue / analogue material property data. Consequently here, building on a series of previous in-house studies [1, 3, 9-14], data on the high strain-rate response of a wide range of

(ballistic) tissue analogues representing all key components of a mammalian limb structure are collectively reported for the first time. This paper is designed to bring together dynamic material property data on a relatively complete selection of potential tissue simulants – with data from previous publications by a selection of the authors re-visited and combined with recent experimental results. Essentially, Hugoniot equation-of-state data (U_s-u_p; P-v) derived from plate-impact experiments [15, 16], which has the potential to serve as feedstock materials data for hydrocode simulations of ballistic impact events, is reported. A total of seven analogues are discussed which are often employed as monolithic simulant materials. These cover epithelial, connective, muscular and simulated skeletal materials, allowing a focus on the classification of the behaviour of differing simulants into groups that exhibit a similar response under high strain-rate loading.

2. Material Properties

A total of seven tissue analogues representative of each of the main constituent elements of biological systems have been considered in this study. A brief background on each material, along with key elastic properties, is presented in Table I. In each case, the tissue simulants are divided into one of four categories: epithelial (lining); connective (providing an interface between differing tissue groups); muscular, or; skeletal (supporting) tissues [17]. Where appropriate, reference to previous work on these simulant materials is also included.

Table I. Key tissue analogue material data.

Material	Key features	Key elastic properties
Epithelial tissue analogues		
Gelatin	(1) Allows water to be cast in a gelatinous (solid) state; behaviour heavily dependant on gel concentration. Here, 250 bloom porcine gelatin (Weishardt International, France) mixed to 25 wt.% at 60 ºC, before cooling to room temperature. (2) Behaves as an elastomer on impact. (3) simulates cavity formation in tissue (initial temporary cavity analogous to the area of peripheral damage around a gunshot wound; final smaller permanent cavity corresponding to the area of crushed tissue ahead of a penetrating projectile) [2].	$\rho_0 = 1.06 \pm 0.01$ g/cc $c_l = 1.48 \pm 0.06$ mm/μs $c_s = 0.33$ mm/μs (*calc.*) $\nu = 0.47$ (*est.)* K = 2.17 GPa (*calc.*)
Sylgard®	Cross-linked silicone rubber, with both linear [18, 19] and non-linear [10] behaviour in the U_S-u_P plane previously observed under shock loading	$\rho_0 = 1.01 \pm 0.01$ g/cc $c_l = 1.10 \pm 0.02$ mm/μs $c_s = 0.57 \pm 0.02$ mm/μs $\nu = 0.32$ (*calc.*) K = 0.78 GPa (*calc.*)
Ballistic Soap	(1) Long-chain backbone structures with active polar "heads". (2) Plastic behaviour under impact, producing permanent cavities of comparable extent to temporary cavities in gelatin [20]. (3) Previously derived non-linear Hugoniot equation-of-state in the U_s-u_p plane [3].	$\rho_0 = 1.11 \pm 0.00$ g/cc $c_l = 1.67$ mm/μs $c_s = 0.69$ mm/μs (*calc.*) $\nu = 0.40$ (*est.*) K = 2.39 GPa (*calc.*)
Perma-Gel®	(1) A commercially available synthetic (polymer-based) gel. (2) Chemically stable at room temperature. (3) Closely simulates 10 wt.% ordnance gelatine in terms of ballistic properties [12, 21, 22].	$\rho_0 = 0.56 \pm 0.01$ g/cc $c_l = 1.42 \pm 0.06$ mm/μs $c_s = 0.38 \pm 0.06$ mm/μs $\nu = 0.46$ (*calc.*) K = 1.03 GPa (*calc.*)
Connective tissue analogues		

Lard	(1) Proposed adipose simulant; complex long-chain structure consisting of glycerol units and attached fatty acids. (2) Commercially available; manufactured by Matthews Foods plc and retailed by the Co-operative® Food Group as "Fresh Fields Lard".	$\rho_0 = 0.95 \pm 0.01$ g/cc $c_l = 1.51 \pm 0.10$ mm/μs $c_s = 0.36$ mm/μs (*calc.*) $\nu = 0.47$ (*est.*) K = 2.00 GPa (*calc.*)
Muscular tissue analogues		
Porcine muscle tissue	Experimental data on both commercially sourced gammon and Middle-White longissimus dorsi porcine muscle tissue is reproduced here (with elastic data for the un-altered material quoted from Ref. [9]).	$\rho_0 = 1.09 \pm 0.00$ g/cc $c_l = 1.93 \pm 0.03$ mm/μs $c_S = 0.89 \pm 0.10$ mm/μs $\nu = 0.36$ (*calc.*) K = 2.90 GPa (*calc.*)
Skeletal tissue analogues		
Synbone®	Polyurethane-based synthetic bone with a bi-model (ca. 50 and 100-mm diameter) porous internal structure. Used as a commercial bone simulant for medical training applications. Available in a variety of configurations ranging from planar sheets through to spherical 'skull-like' structures.	$\rho_0 = 0.77 \pm 0.10$ g/cc $c_l = 1.75 \pm 0.13$ mm/μs $c_S = 0.71 \pm 0.10$ mm/μs $\nu = 0.40$ (*calc.*) K = 1.84 GPa (*calc.*)

3. Experimental Method

Data presented in this paper was gathered via a series of plate-impact experiments [15-16]. A 50-mm bore single-stage gas-gun [23] was employed to impact tissue analogue targets in the velocity regime 75 to 993 m/s with Cu and Al 6061 flyer plates. Targets were carefully prepared with all impact and target surfaces perpendicular to the impact axis finished to a tolerance of ≤5 μm to ensure they were parallel with each other. This allowed all elements of the projectile's surface to make contact with the target essentially simultaneously. In turn, inertial confinement of the target material constrained radial material flow, thereby impacting a planar (1D) strain (but not stress) loading into the target, establishing the stress (σ) / strain (ε) states detailed in Equations 1 and 2.

$$\varepsilon_x \neq \varepsilon_y = \varepsilon_z = 0$$

Equation 1

$$\sigma_x \neq \sigma_y = \sigma_z = 0$$

Equation 2

Where the subscripts '*x*' and '*y*' denote the condition along and orthogonal to the impact axis respectively.

Longitudinal embedded manganin stress gauges of type LM-SS-125CH-048 manufactured by Vishay Micro-Measurements, USA were employed to monitor shock propagation, with interpretation based on Ref. [24]. While the specifics of target construction varied with each target material, and are reported elsewhere [1, 3, 9-14], the generic arrangement employed was in line with that illustrated in Figure 1.

---- Figure 1 near here ----

4. Results and Discussion

For the epithelial, connective and muscular materials, data employed here has been previously published elsewhere [1, 3, 9-12]; whereas for the Synbone®, new experimental data is presented alongside previously published data [13, 14] re-interpreted in the light of the recent additional results. The resultant experimental data for Synbone® is presented in Table II, with maximum potential calculated errors (derived following the approach detailed in Ref. [25]) included for reference.

Table II. Summary of plate-impact experimental results for Synbone®.

Impact velocity (m/s)	Flyer type / thickness (mm)	u_p (mm/μs)	U_s (mm/μs)	σ_x / P (GPa)
304	Al / 10	0.279 ± 0.001	1.015 ± 0.069	0.326 ± 0.029
340	Al / 10	0.312 ± 0.001	1.097 ± 0.040	0.399 ± 0.029
381	Al / 10	0.351 ± 0.001	1.109 ± 0.028	0.459 ± 0.015
391	Cu / 10	0.383 ± 0.001	1.090 ± 0.060	0.538 ± 0.013
455	Cu / 10	0.445 ± 0.001	1.194 ± 0.136	0.750 ± 0.017
504	Cu / 10	0.493 ± 0.001	1.214 ± 0.060	1.603 ± 0.121
584	Cu / 10	0.569 ± 0.000	1.361 ± 0.033	1.121 ± 0.083
640	Cu / 10	0.621 ± 0.311	1.508 ± 0.072	0.767 ± 0.226
745	Cu / 10	0.717 ± 0.001	1.834 ± 0.068	2.200 ± 0.020
845	Al / 10	0.761 ± 0.002	1.884 ± 0.055	1.803 ± 0.071
962	Cu / 5	0.918 ± 0.002	2.259 ± 0.098	2.483 ± 0.337

Typical gauge traces for the six potential bulk analogue materials considered are presented in Figure 2; i.e. all tissues considered except for Synbone®. Based on knowledge of gauge separation (e.g. target thickness), arrival times at successive gauges allowed direct calculation of shock velocity for given impact conditions. In each case in Figure 2, the amplitude of the rear gauge trace has been normalised to that of the front gauge via an impedance match taking into account the impedance of the backing PMMA [25, 26].

---- Figure 2 near here ----

All of the traces presented in Figure 2 exhibit a number of similarities, namely:

1. a rapid (between 100-200 ns) rise in stress on shock arrival
2. evidence of ringing – tentatively attributed to electrical effects due to its high frequency – as the system reaches a peak stress
3. decay from the initial peak to a plateau in stress (nominally constant, with a small gradient in some cases)
4. either tensile release arrival at the front gauge followed by unloading and then shock arrival, leading (typically without ringing) to a similar sequence of events at the rear surface gauge, or vice-versa (e.g. for Ballistic Soap in Figure 2(c), where target geometry led to rear gauge shock arrival before release arrival at the front gauge)

Despite these similarities, some differences between the different sets of gauge traces are apparent. Several of these are simply a function of the target arrangement – whereas others are likely linked to underlying material response.

One key difference is the presence of re-loadings during the initial stress pulse (and corresponding events on the rear surface gauges) in Figures 2(a), (c) and (d) for Gelatin, Ballistic Soap and Sylgard® respectively. These can be shown to be a function of the nature of the target configurations – with relatively high shock speeds and thin target constructs leading to re-loading before release arrival. More fundamentally, even though the structure of the initial input pulse (i.e. a square-wave) was nominally similar in each case, the resultant front surface gauge traces (representing stress in the target material) have markedly different profiles. Interestingly, relatively little initial ringing is apparent following the initial rise in Soap in Figure 2(c) as opposed to the other target materials considered. This appears to correlate to the presence of a ramp to the stress plateau behind the initial shock for Soap as opposed to an overshoot in the other cases. Such behaviour has been linked elsewhere to underlying material structure, albeit in metals and in the lateral rather than longitudinal plane [27]. As such ramping is not observed in the front gauge traces associated with the polymeric simulants Perma-Gel®, Sylgard® and lard, entanglement of polymer chains is probably not influencing this response [28-30].

Instead, it is tentatively postulated that this behaviour arises due to the polar nature of Soap molecules acting on compression act to repel each other. This repulsion would increase in magnitude with the degree of compression, potentially leading to the observed damped final rise and subsequent reduced ringing.

In addition, it is worth highlighting the unusual form of the rear surface trace in Figure 2(d) for Sylgard® as well as that for muscle tissue in Figure 2(f). This rear surface trace exhibits a ramped rise to the final Hugoniot stress. This is tentatively attributed here to pore (air entrapment from Sylgard® preparation) collapse (while some ramping is apparent on the front gauge this is minimal – meaning that as observed behind the target, the phenomena is almost certainly a result of its inherent structure). Essentially, such behaviour is indicative of an increase in apparent strength – or resistance to compression. In this case, this is likely a result of the pores beginning to collapse as the leading edge of the shock propagates through the Sylgard®. This would lead to an increase in material density – and therefore impedance, meaning that this compressed material would inevitably be able to higher stress.

Synbone® is considered separately here due to its more complex (porous) structure. Traces are presented in Figure 3 covering a variety of different loading pressures / velocities. These traces, as well as exhibiting the features highlighted in Figure 2, also show a couple of interesting – and unique – points. In all cases the relatively short loading duration compared to the traces presented in Figure 2 for the other six analogue materials is the result of the limited target thicknesses commercially available. Although here, even though the release arrives in <1μs, the eventual rapid rise at the rear surface suggests that a shock was still established in the target material, validating its inclusion in subsequent data analysis.

In all cases the main rise on the rear gauge traces presented in Figure 3 are preceded by a relatively low amplitude and long rise time (relative to the front surface gauge) feature. This initial element of the rise possessed a mean amplitude of 0.082 GPa with a standard deviation of 0.015 GPa. As the velocity increased, whilst the amplitude remained relatively constant, this feature was observed to steadily decrease in duration. Combined, this suggests that the initial ramp is an elastic precursor – with this being close to overdriven at higher velocities – e.g. Figure 3(c). The velocity of

this feature was found to be slightly less than that of the longitudinal sound speed for 100% dense polyurethane of 2.39 mm/μs [26]; e.g. it ranged from 1.82 to 2.03 mm/μs for the three cases show in Figure 3. It is postulated that this precursor represents an elastic wave travelling through the polyurethane matrix, with the lower velocity compared to 100% dense polyurethane – and associated scatter in measured values – likely attributable to the tortuous path which such waves would have to follow through the structural elements of the porous Synbone®.

---- Figure 3 near here ----

Following on from the initial precursor, the rear surface gauges for Synbone® targets were consistently observed to rise to a peak relatively slowly. This ramped response is attributed here to the final collapse of the pores present within the material (with initial collapse having started on shock arrival), before the compressed material subsequently 'shocks-up' to the final Hugoniot stress. This unusual collapse – likely linked to the relatively high material porosity – was also apparent in optical analysis of recovered samples. For example, Figure 4 illustrates the effect of shock loading at nominally 228 m/s with an Al flyer on the bulk of a Synbone® sample. As shown in Figure 3(b), the pores can be observed to have collapsed along the impact axis, with fracture consistently occurring at the edges of the pores perpendicular to the loading axis. It is interesting to note that this failure appears to propagate in nominally lateral planes across the material.

Further, significant oscillations were also apparent on all Synbone® shots. These were most prominent on the front surface gauge and were likely a function of the incident shock reflecting back / forth from pores just below the target material surface. As an example, over the first half micro-second of the front gauge trace in Figure 3(c), these oscillations are found to have frequencies nominally in the range 10 to 25 MHz. Assuming an elastic sound speed of approximately 2 mm/μs, this corresponds to

feature sizes of nominally 200 to 80 microns respectively – consistent with the range of pore sizes observed in Figure 4.

---- Figure 4 near here ----

In terms of shock response, Hugoniot equations-of-state were measured / calculated for all materials considered here in the U_s-u_p plane – e.g. for both the Dermal (epithelial, connective and muscular) and Skeletal simulants. These are illustrated in Figure 5 as lines-of-best fit through the experimental data, with the associated equations (non-linear in all cases except lard, muscle and gelatin) detailed in Table III. Individual data points represent shock states derived from plate-impact experiments. The impedance matching technique [26] was employed to calculate particle velocities based on the known Hugoniot equation-of-state and impact velocity of the flyer plate, as well as the measured shock velocities derived from knowledge of shock arrival times at the front and rear of targets of known thickness in line with Figure 1(b). The best-fit curves (derived using in-built least-squares-fitting algorithms in Microsoft Excel®) consequently represent the Hugoniot equations-of-state (loci of obtainable shock states from ambient conditions).

---- Figure 5 near here ----

From Figure 5 it is immediately apparent that the tissue simulants considered fall into a number of different, discrete, groups. Considering first the six dermal (bulk) materials separately to the skeletal analogue Synbone®, behaviour at low impact

(particle) velocities also appear to be different to that at higher velocities. In the low velocity (broadly $u_p < 0.6$ mm/μs) regime, the epithelial simulants gelatin and Perma-Gel®, as well as the connective material lard and the muscular tissue analogue all behave in a similar manner. Whereas Sylgard® and ballistic soap exhibit markedly different responses both to this group and to each other. At elevated impact velocities, there appears to be a greater convergence in terms of material response in all cases – in particular in terms of the equation-of-state for the ballistic soap converging with those of the other five dermal simulant materials considered. This convergence is likely attributable to the underlying polymeric-like nature of the various materials. Essentially it is postulated that at elevated particle velocities (and therefore pressures) the materials will likely be compressed sufficiently that they will exhibit similar densities / impedances – thereby sustaining similar shock velocities under otherwise equivalent loadings.

However, it is notable that despite the convergence of the epithelial, connective and muscular tissue simulant Hugoniot equations-of-state at higher impact velocities, there is still a marked separation in terms of absolute shock velocities for a given particle velocity. In particular, gelatin and Sylgard® appear to exhibit much lower shock velocities than the other materials, with a convergence only at higher particle velocities. While their comparable densities (Table II) might suggest a similarity in response (e.g. hydrodynamic-like behavior – in line with the fact that gelatin is by definition simply a gelled fluid), their differences in structure – combined with P-v response (see Figure 6) make this unlikely. Instead, it seems likely that the convergence in this regime may be coincidental – with supported shock velocities for Sylgard® likely continuing to trend upwards at even higher flyer impact velocities than those accessible with the equipment employed here. Finally, it is worth noting that Synbone exhibits a very different U_s-u_p response to the bulk materials – with the increasing rate of enhancement to shock velocity as the particle velocity increases likely attributable to pore collapse / consequent enhancement in material density.

The equations for the resultant best-fit Hugoniot curves plotted through experimental data points are presented in Table III along with corresponding residual R^2 values. For clarity error bars have been omitted. Experimental data is available in the original sources for the experimental data employed / Table II for Synbone®. In

addition, references to the published sources of experimental data are included. For all seven analogue materials considered, best-fits were calculated with both linear and polymeric (quadratic) forms of type $U_s = c_0 + Su_p$ and $U_s = c_0 + Su_p + S'u_p^2$ respectively. It is interesting to note that for the PermaGel® and Synbone® the non-linear curves produced a much better fit to the experimental data, whereas in the other cases the linear fit was more effective. Such non-linear responses have been linked elsewhere to polymeric behaviour – with the non-linearity arising from the different strengths of inter- and intra-chain bonds and the resultant differential failure of these bonds under high strain-rate loading [31].

Table III. Experimental and calculated Hugoniot equations-of-state.

Material	**Equations-of-state**	**R^2**
Gelatin	$U_s = 1.57 + 1.77u_p$	0.95
	$U_s = 1.55 + 1.87u_p - 1.12u_p^2$	0.95
Lard	$U_s = 1.56 + 2.50u_p$	0.9857
	$U_s = 1.42 + 2.91u_p - 0.26u_p^2$	0.9741
Ballistic	$U_S = 2.05 + 1.77u_P$	0.9808
Soap	$U_s = 1.94 + 2.52u_p - 0.81u_p^2$	0.9936
Sylgard®	$U_s = 1.03 + 2.45u_p$	0.9855
	$U_s = 0.96 + 3.03u_p - 0.68u_p^2$	0.9898
Perma-Gel®	$U_s = 1.91 + 1.81u_p$	0.9329
	$U_s = 1.20 + 4.60u_p - 2.42u_p^2$	0.9784
Muscle	$U_s = 1.73 + 1.86u_p$	0.9867
Tissue	$U_s = 1.74 + 1.82u_p + 0.04u_p^2$	0.9867
Synbone®	$U_s = 0.38 + 1.94u_p$	0.9541
	$U_s = 0.95 - 0.29u_p + 1.92u_p^2$	0.9857

In the U_s-u_p plane, for materials with a linear equation-of-state, the intercept with the ordinate axis typically corresponds to the material's bulk sound speed, whereas the gradient (S) has been linked to material compressibility as the first pressure derivative of the bulk modulus. Essentially, higher values of 'S' appear to correspond to higher material compressibility [28-30]. To this end, in terms of compressibility the data

presented in Table III (for linear fits) suggests that the tissue analogues considered here may therefore be ranked as follows: compressibility of…. gelatin ≈ Ballistic Soap < Perma-Gel® ≈ muscle tissue < Synbone® < Sylgard® < Lard. The relatively incompressible nature of Gelatin is unsurprising – suggesting that the material is essentially behaving like water under impact. The comparable compressibility of Ballistic Soap is more surprising, however – suggesting that the Soap's polar-headed molecules do not influence compressibility. For comparison, as detailed later in Figure 6, in the P-v, plane, Ballistic Soap appears to show a markedly different resistance to compression as opposed to gelatin. This discrepancy is tentatively attributed here to the fact that, in reality, as detailed in Table III, Ballistic Soap demonstrates a non-linear response in the U_s-u_p plane (evidenced by a markedly higher magnitude value of 'S' of 2.52 as opposed to 1.77 when non-linear and linear fits are considered respectively). In turn, the increase in compressibility moving from Perma-Gel® to Sylgard® and lard is likely linked to a corresponding increase in underlying polymeric material complexity. Essentially, it is postulated – in line with work on the influence of polymeric chain side groups on shock response elsewhere [28-30] – that steric effects would have led to enhanced resistance to compression as structural elements become more complex.

Synbone® is a slightly different case to the dermal (bulk) tissue analogues in that the underlying material is polyurethane. For comparison, the corresponding equation-of-state for solid polyurethane (ρ_0 = 1.264 g/cc) in the U_s-u_p plane is $2.45 + 1.58u_p$ [26] within the shock regime in question. Unsurprisingly, this suggests that solid polyurethane is significantly less compressible than the porous Synbone® (where the linear best-fit curve from Table III is considered). Further, it is interesting to note when the polynomial (non-linear) best fit curve from Table III is compared to those (both linear and non-linear) for the dermal analogues, that the 'S' term for Synbone® has a negative coefficient (as opposed to positive for all other cases). This is likely a function of the porous nature and consequent multi-phase collapse of the material under increased loading. The link between compressibility and bulk modulus is normally only valid for linear equations-of-state [28-30]. However, as shown in Figure 5, an increase in gradient in the U_s-u_p plane as particle velocity (and therefore loading rate) increases occurs for Synbone®. Physically, this suggests reduced

compressibility; e.g. as the pores are taken up / collapse, material compaction accelerates and compressibility deceases.

Measured / calculated experimental data derived from plate-impact experiments conducted using the six dermal simulant materials investigated are presented in Figure 6 in the P/σ_x -v plane. Volumes were calculated from the measured U_s-u_p data presented in Figure 5 / Table III via Equation 3 [16], with pressures / stresses measured directly in the tested materials via embedded Manganin gauges (see Figure 1). Alongside the experimental data, hydrodynamic curves calculated using Equation 4 [16] are also presented for comparative purposes.

$$v = v_0 [(U_s - u_p) / U_s]$$

Equation 3

$$P = \rho_0 U_s u_p$$

Equation 4

---- Figure 6 near here ----

From Figure 6 it is apparent that the six dermal (epithelial, connective and muscular) simulants considered here behave in markedly different manners under shock. The different analogue materials separate into two distinct groups which each subsequently converge in terms of material response at elevated pressures / stresses. The first group is gelatin and Sylgard®, with the second comprising muscle, Perma-Gel®, Soap and lard. Enhanced resistance to compression is evidenced by both the convergence of the Hugoniot data at higher apparent stresses for the second group of

materials (consistent with the convergence of U_s-u_p data in Figure 5), as well as deviation of the highest amplitude experimental data points above the corresponding hydrodynamic curves for the Soap, Perma-Gel® and muscle (in line with Equation 5 [10, 34]).

$$\sigma_x = P + (4/3) \times \tau_{max}$$

Equation 5

Where P is the hydrostatic pressure and τ_{max} is the maximum shear strength of the target material.

Such behaviour suggests a continued residual material strength despite the relatively high loading stresses, a result which is consistent with the proposed steric effect for Soap detailed in the discussion of Table III. In the case of the muscular material it is postulated that this effect derives from the sinuous nature of the medium. However, for the other four simulant materials considered in Figure 6, instead of such a deviatoric response, the experimental data is to a large extent co-incident with the corresponding hydrodynamic curves.

The data presented in Figure 6 excludes that for the skeletal simulant material, Synbone®. When this data is included – as shown in Figure 7 – a notable difference in material response is immediately apparent.

---- Figure 7 near here ----

The compression curve for the Synbone® data presented in Figure 7 is based on Equations 4 and 6 [35]. The polynomial best-fit presented in Table III was applied to calculate P, where Pc is the cold Hugoniot curve (assumed to be the Hugoniot here)

and $K = 2\Gamma_0 + 1$ – with Γ (Grünessian gamma) taken to have a value of 1.55 – namely that of polyurethane [36].

$$P_H(v, v_0) = [(K - 1)Pc(v) - 2\varepsilon_0(v) / v] / [(K - v_0) / v]$$

Equation 6

Good agreement is observed between the compression and experimental data. Further, there appears to be evidence that the Synbone® data is trending back towards the response of polyurethane – the material from which it comprised and whose bulk Hugoniot equation-of-state is included here for comparison [26].

Unsurprisingly, the results presented here suggest that under impact Synbone® is behaving as a compacting porous material. The data presented in Figure 7 appears to suggest that at higher pressures a slight increase in volume is occurring. While potentially simply a function of inherent errors on the measured data, such a response could potentially be attributed to thermal thermal effects as pores collapse leading to a reduction in density – and therefore an increase in volume. Such behaviour (namely an inversion of the Hugoniot equation-of-state in the P-v plane) in a porous material was described by Zel'dovich, and, Raizer [35]. Overall, from Figure 7, it is immediately clear that in addition to the two different groups of analogues with similar high strain-rate behaviours previously identified (Soap, lard and Perma-Gel® in the first instance and gelatin and Sylgard® in the second), the response of Synbone® to impact loading is such that an additional sub-set of data is required.

5. **Conclusions**

In this paper shock data (Hugoniot equations-of-state) for a selection of seven tissue analogues (four epithelial, one connective, one muscular and one skeletal, from a combination of new experiments and previous work by the authors) is collectively presented for the first time. From material response in both the U_s-u_p and P-v planes it is apparent that even within the single epithelial tissue analogue category, analogue materials behave in demonstrably different manners under high strain-rate (shock) loading. In particular, it has been observed that the epithelial simulants Ballistic Soap,

Perma-Gel® and the connective simulant Lard exhibit similar behaviours in the P-v plane. Whereas gelatin and Sylgard® sit within a second category which exhibits a lower resistance to compression under a given impact, while the skeletal analogue Synbone® shows a collapse indicative of a porous structure.

Thus, the results presented demonstrate that tissue analogues behave in fundamentally different manners under high strain-rate loading. In addition, it is apparent that tissue simulants with fundamentally different applications can exhibit an otherwise similar hydrodynamic response, for example, the bulk and brain tissue simulants gelatin and Sylgard®, respectively. Consequently, it is suggested that the use of a single tissue analogue would be inherently inaccurate when studying high strain-rate / ballistic effects. Instead, it is proposed that a composite approach – with full underlying understanding of the individual tissue components responses – would provide a more realistic simulant solution.

6. **Acknowledgements**

The authors are grateful to Andrew Roberts of Cranfield University for aid in the experimental work presented in this paper. In addition, the authors would like to acknowledge the fact that the data on gelatin and ballistic soap was largely derived as part of a PhD research programme involving Dr Christopher Shephard, with that for muscle tissue derived during the PhD research programme of Dr James Wilgeroth (both at Cranfield University); while that for Synbone® was largely gained during a recent Forensics MSc conducted by one of the current authors, Ms Brianna Fitzmaurice.

7. References

1. Shepherd, C. J., G. J. Appleby-Thomas, P. J. Hazell and, D. F. Allsop. 2009. "The dynamic behaviour of ballistic gelatin," in *Proceedings of the American Physical Society Topical Group on Shock Compression of Condensed Matter*, M. L. Elert, W. T. Buttler, M. D. Furnish, W. W. Anderson, and W. G. Proud. eds. AIP, Melville, New York, pp. 1399-1402.

2. Nicholas, N. C. and, J. R. Welsch. 2004. "Ballistic Gelatin," Institute for Non-Lethal Defense Technologies Report, Applied Research Laboratory, The Pennsylvania State University, USA.
3. Shepherd, C. J., G. J. Appleby-Thomas, J. M. Wilgeroth, P. J. Hazell and, D. F. Allsop. 2011. "On the response of ballistic soap to one-dimensional shock loading," *Int. J. Impact Engng.*, 38(12): 981-988.
4. Comley, K. and, N. A. Fleck. 2010. "The toughness of adipose tissue: measurements and physical basis," *J. Biomech.*, 43: 1823–1826.
5. Jussila, J., A. Leppäniemi, M. Paronen and, E. Kulomäki. 2005. "Ballistic skin simulant," *Forensic Sci. Int.*, 150: 63-71.
6. McElhaney, J. H. 1966. "Dynamic response of bone and muscle tissue," *J. Appl. Physiol.* 21: 1231-1236.
7. Ural, A., P. Zioupos, D. Buchanan and, D. Vashishth. 2011. "The effect of strain rate on fracture toughness of human cortical bone: A finte element study." *J. Biomed. Mater.* 4: 1021-1032.
8. Van Sligtenhorst, C., D. S. Cronin and, G. Wayne Brodland. 2006. "High strain rate compressive properties of bovine muscle tissue determined using a split Hopkinson bar apparatus," *J. Biomech.* 39: 1852-1858.
9. Wilgeroth, J. M., P. J. Hazell and, G. J. Appleby-Thomas. 2012. "On the behaviour of porcine skeletal muscle tissue under shock compression," *Int. J. of Impact Engng.*, 50L 83-89.
10. Appleby-Thomas, G. J., P. J. Hazell, R. P. Sheldon, C. Stennett, A. Hameed and, J. M. Wilgeroth. 2014. "The high strain-rate behaviour of selected tissue analogues," *J. Mech. Behaviour of Biomedical Mater.*, 33(1):124-135.
11. Appleby-Thomas, G. J., P. J. Hazell, J. M. Wilgeroth, C. J. Shepherd, D. C. Wood and, A. Roberts. 2011. "On the dynamic behaviour of three readily available soft tissue simulants," *J. Appl. Phys.*, 109: 084701.
12. Appleby-Thomas G. J., D. C. Wood, A. Hameed, J. Painter, V. Le-Seelleur and, B. Fitzmaurice. 2016. "Investigation of the high-strain rate (shock and ballistic) response of the elastomeric tissue simulant Perma-Gel®", *Int. J. of Impact Engng.*, 94: 74-82.

13. Appleby-Thomas G. J., B. Fitzmaurice, A. Hameed, D. C. Wood, M. C. Gibson and, J. Painter. 2017. "The shock response and suitability of Synbone® as a tissue simulant", in Proceedings of the American Physical Society Topical Group on Shock Compression of Condensed Matter 2015, AIP Conf. Proc., Vol. 1793, 140009 1-5.
14. Appleby-Thomas G., A. Hameed, B. Fitzmaurice, J. Painter and, D. Wood. 2016. "On the selection of tissue simulants for ballistic testing", in Proc. – 29th Int. Symp. on Ballistics, Vol. 2, 2367-2377.
15. Field, J. E., S. M. Walley, W. G. Proud, H. T. Goldrein and, C. R. Siviour. 2004. "Review of experimental techniques for high rate deformation and shock studies," *Int. J. Impact Engng.*, 30: 725-775.
16. Meyers, M. A. 1994. "Dynamic Behavior of Materials," John Wiley & Sons, Inc., New York, USA.
17. Roberts, M. V. B. 1973. "Biology. A Functional Approach," Cox and Wyman Ltd., London, UK.
18. Millett, J. C F, G. Whiteman, S. M. Stirk and, N. K. Bourne. 2011. "Shear strength measurements in a shock loaded commercial silastomer," *J. Phys. D: Appl. Phys.*, 44(18):185403.
19. Winter, R. E., G. Whiteman, G. Haining, D. A. Salisbury and, K. Tsembelis. 2003. "Measurement of Equation of State of Silicone Elastomer," in Proceedings of the American Physical Society Topical Group on Shock Compression of Condensed Matter, M. D. Furnish, Y. M. Gupta, and J. W. Forbes. eds. AIP, Melville, New York, pp. 679-682.
20. Rutty, G. N., P. Boyce, C. E. Robinson, A. J. Jeffery and, B. Morgan. 2008. "The role of computed tomography in terminal ballistic analysis," *Int. J. Legal Med.* 122: 1-5.
21. Mabbott, A., D. J. Carr, S. Champion, C. Malbon, C. Tichler. 2013. "Comparison of 10% Gelatine, 20% Gelatine and Perma-Gel^{TM} for Ballistic Testing," Proc. of the 27th Int. Symposium on Ballistics, Freiburg, Germany, pp. 648-654.
22. Ryckman, R. A., D. A. Powell, A. J. Lew. 2011. "Ballistic Penetration of Perma-Gel," in Proceedings of the American Physical Society Topical Group on Shock Compression of Condensed Matter, AIP, Chicago, Illinois, pp. 143-148.

23. Bourne, N. K. 2003. "A 50 mm bore gas gun for dynamic loading of materials and structures," *Meas. Sci. & Tech.*, 14,: 273-278.
24. Rosenberg, Z., D. Yaziv and, Y. Partom. 1980. "Calibration of foil-like manganin gauges in planar shock wave experiments," *J. Appl. Phys.*, 51: 3702-3705.
25. Appleby-Thomas, G., P. J. Hazell, C. Stennett, G. Cooper, K. Herlaar and, A. M. Diederen. 2009. "Shock propagation in a cemented tungsten carbide," *J. Appl. Phys.*, 105(6): 064916.
26. Marsh, S. P. 1980. "LASL Shock Hugoniot Data," University of California Press, Ltd., London, UK.
27. Bourne, N. K., G. T. Gray III and, J. C. F. Millett. 2009. "On the shock response of cubic metals," *J. Appl. Phys.*, 106:091301.
28. Bourne, N. K. and, J. C. F. Millett. 2008. "On the influence of chain morphology on the shock response of three thermoplastics," *Metallurgical and Mater. Trans. A: Physical Metallurgy and Mater. Sci.*, 39(2):266-271.
29. Millett, J. C. F., N. K. Bourne and, G. T. Gray III. 2004. "The response of polyether ether ketone to one-dimensional shock loading," *J. Phys. D: Appl. Phys.*, 37(6):942-947.
30. Bourne, N. K. and, J. C. F. Millett. 2008. "Tacticity in shocked polymer hydrocarbons," *J. Mater. Sci.*, 43(1):185-189.
31. Porter, D. and, P. J. Gould. 2006. "A general equation of state for polymeric materials," *J. Phys. IV*, 134: 373-378.
32. Davison, L. and, R. A. Graham. 1979. "Shock Compression of Solids," *Physics Reports (Review Section of Physics Letters)*, 55(4):255-379.
33. Millett, J. C. F., N. K. Bourne, Y. J. E. Meziere, R. Vignjevic and, A. Lukyanov. 2007. "The effect of orientation on the shock response of a carbon fibre-epoxy composite," *Compos. Sci. and Tech.*, 67:3253-3260.
34. Bourne N. K. and, J. C. F. Millett. 2003. "The high-rate response of an elastomer," *Proc. R. Soc. Lond. A*, 459: 567-576.
35. Zel'dovich, Y. B. and, Y. P. Raizer. 2005. "Physics Of Shock Waves And High-Temperature Hydrodynamic Phenomena," Dover Publications Inc., New York, pp. 705–715.

36. Staudhammer, K. P., L. E. Murr and, M. A. Meyers. 2001. "Fundamental Issues and Applications Of Shock-Wave and High-Strain-Rate Phenomena," Elsevier Science Ltd., Oxford, pp. 485-486.

Figures (formatted)

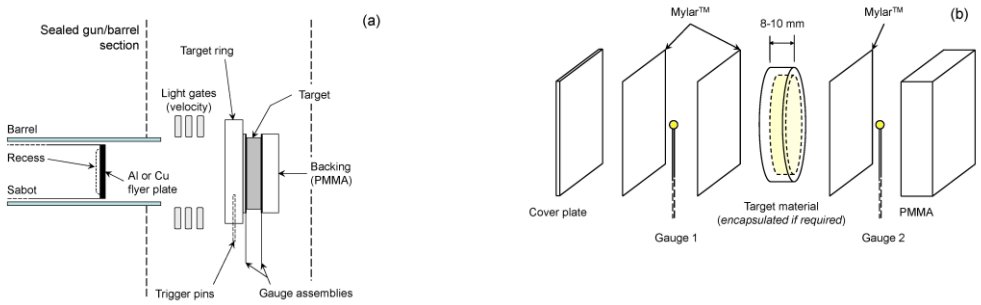

Figure 1. Schematic illustration of plate-impact experimental setup, showing longitudinal target arrangement: (a) mounting configuration; (b) exploded view of target construction.

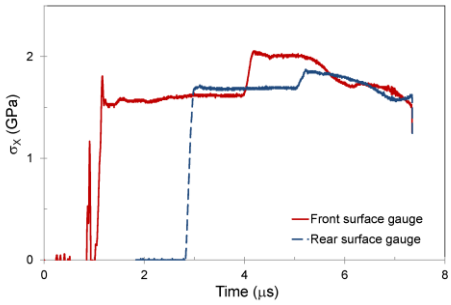

(a) Gelatin: 10-mm Cu flyer @ 604 m/s

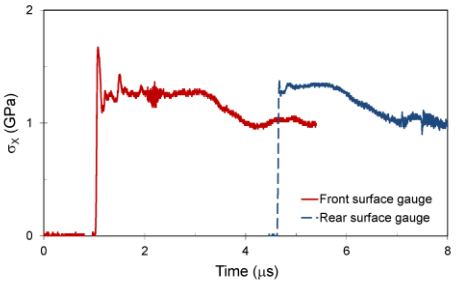

(b) Lard: 10-mm Cu flyer @ 489 m/s

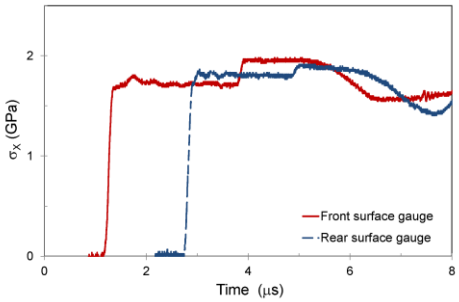

(c) Soap: 10-mm Cu flyer @ 525 m/s

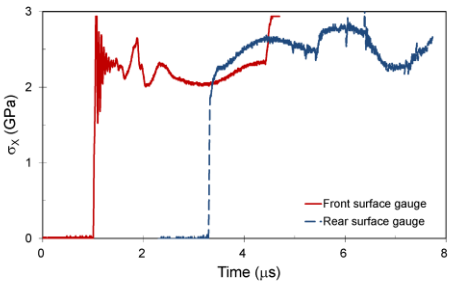

(d) Sylgard®: 10-mm Cu flyer @ 754 m/s

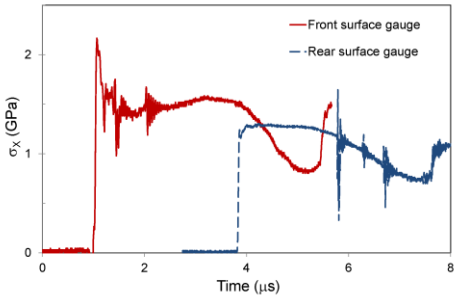

(e) Perma-Gel®: 10-mm Al flyer @ 619 m/s

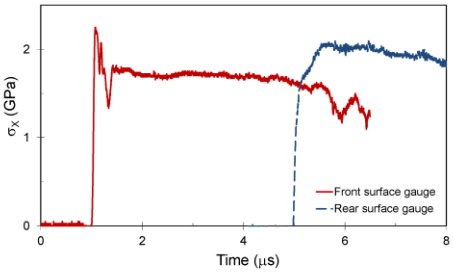

(f) Muscle: 10-mm flyer @ 497 m/s

100816A

Figure 2. Typical longitudinal stress gauge traces for the bulk tissue analogue materials investigated here.

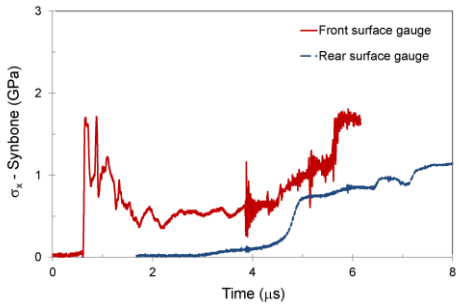

(a) 10-mm Cu flyer @ 504 m/s; $v_{precursor}$ = 2.03 mm/μs

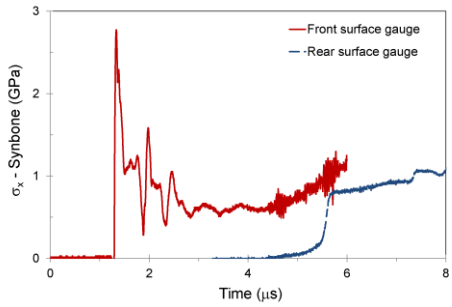

(b) 10-mm Cu flyer @ 584 m/s; $v_{precursor}$ = 1.82 mm/μs

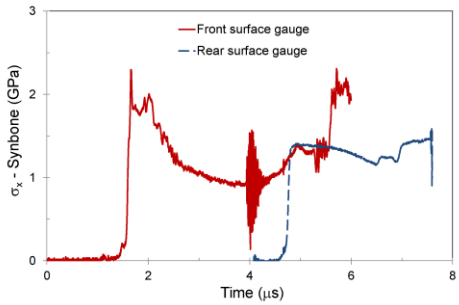

(c) 10-mm Al flyer @ 845 m/s; $v_{precursor}$ = 1.99 mm/μs

Figure 3. Typical gauge traces for three Synbone® plate-impact experiments.

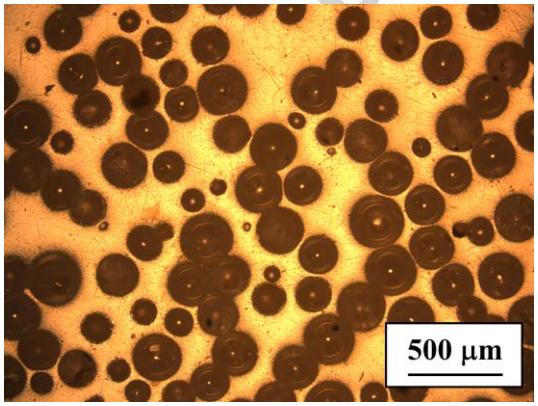

(a) pre-impact

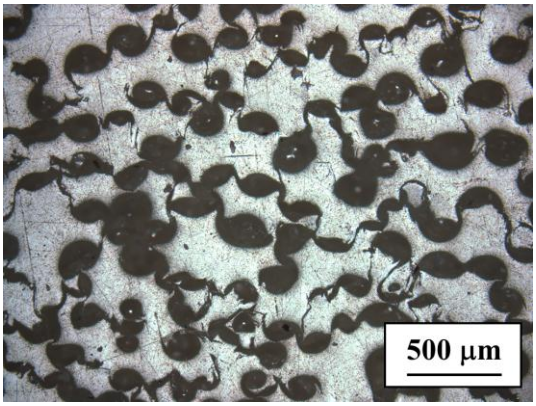

(b) post-impact – 10-mm Al flyer @ 228 m/s

Figure 4. Optical micrographs illustrating the effect of impact on the microstructure of Synbone®, with the loading axis perpendicular to the micrograph for (b).

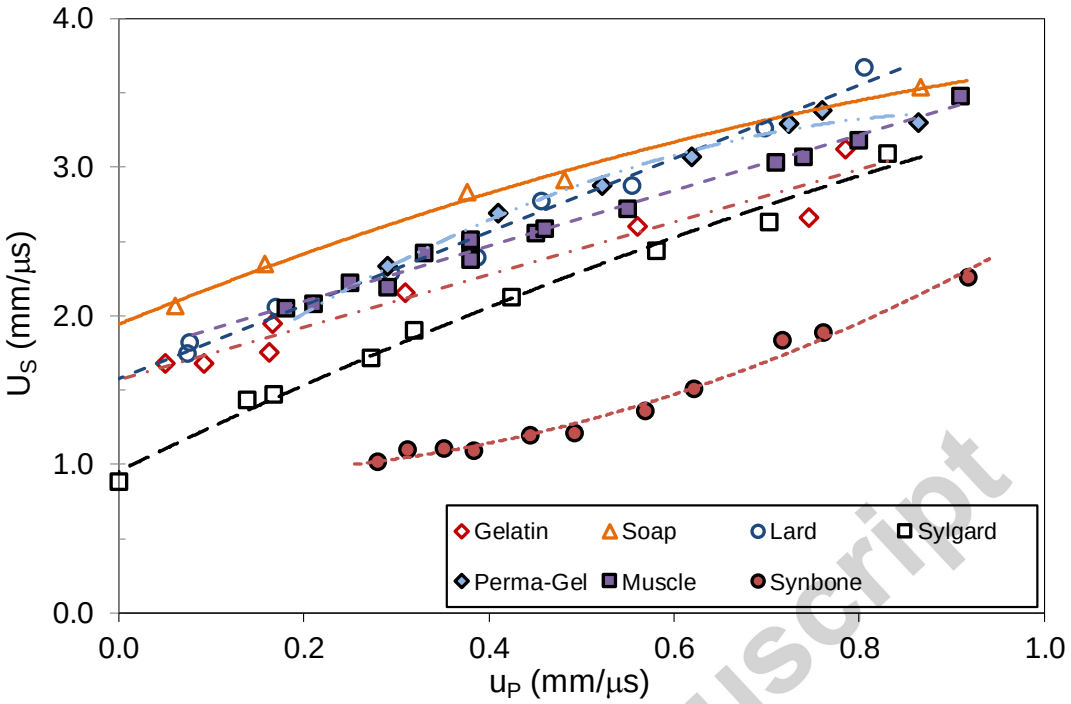

Figure 5. Hugoniot equation-of-state data in the U_s-u_p plane for the tissue analogues considered in this paper with best-fit curves following the equations detailed in Table III.

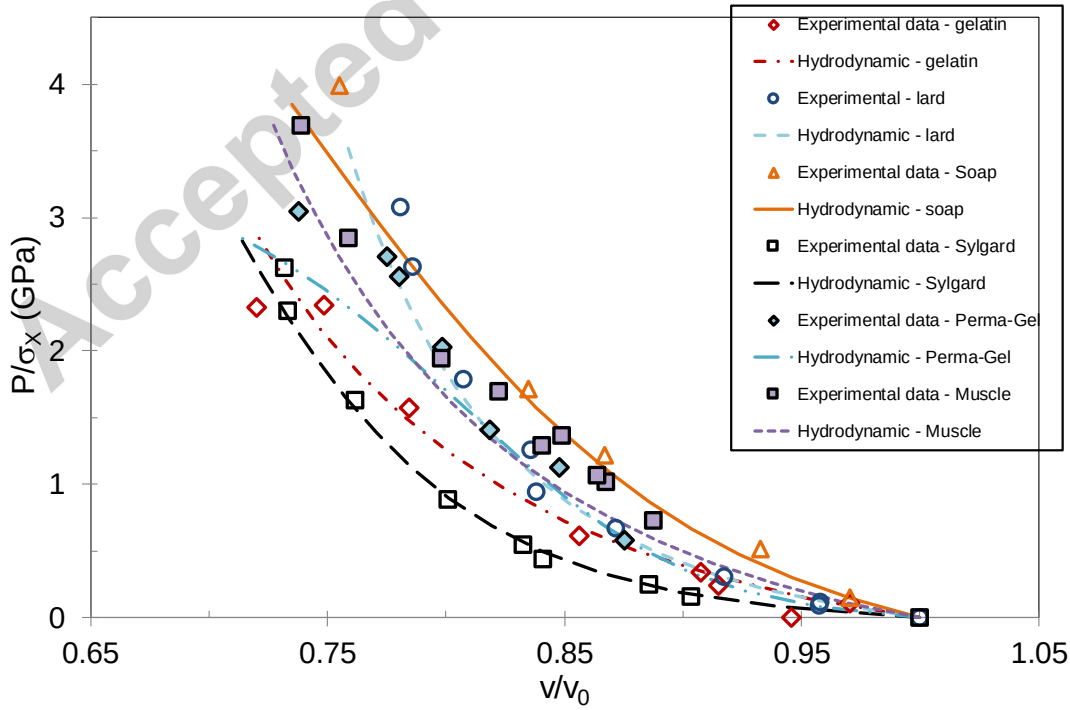

Figure 6. Hugoniot equation-of-state data in the v-P / σ_x plane for the six epithelial, connective and muscular tissue analogues considered.

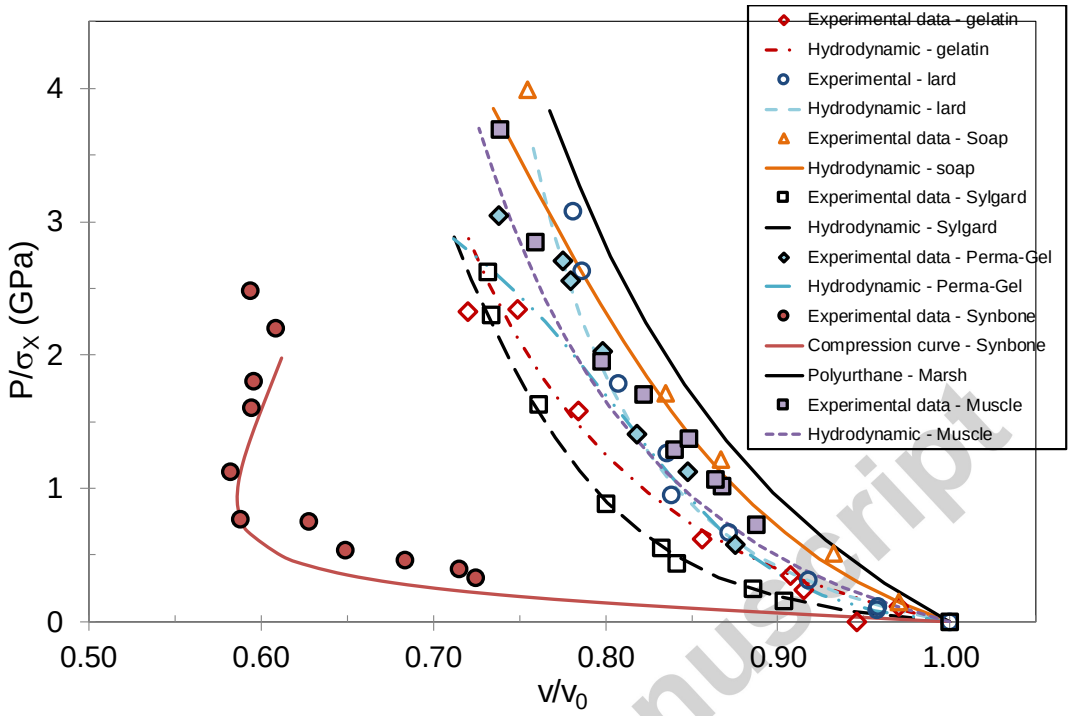

Figure 7. Hugoniot equation-of-state data in the v-P / σ_x plane for the six tissue analogues considered / detailed in Table I.

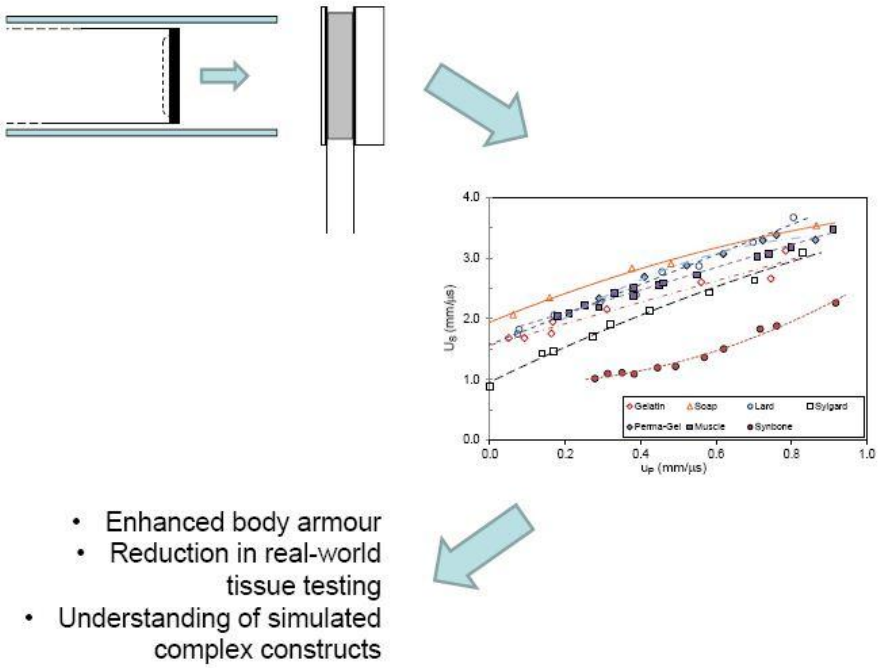

Graphical Abstract

Highlights: On differences in the equation-of-state for a selection of seven representative mammalian tissue analogue materials

- Hugoniot equations-of-state derived for seven mammalian tissue analogues
- Six dermal analogues and one skeletal simulant considered
- Limitations of using monolithic ballistic tissue simulants identified
- Potential route to reduce real-world tissue testing
- Enhanced understanding of simulated complex constructs